Diffusion Limited Photoluminescence Quantum Yields in 1-D Semiconductors: Single-Wall Carbon Nanotubes

Tobias Hertel,[†,*] Sabine Himmelein,[‡] Thomas Ackermann,[§] Dominik Stich,[†] and Jared Crochet[⊥]

[†]Institute of Physical and Theoretical Chemistry & Department of Chemistry and Pharmacy, University of Würzburg, D-97074 Würzburg, Germany, [‡]Institute of Organic Chemistry, University of Münster, 48149 Münster, Germany, and [§]Institute of Inorganic Chemistry, University of Köln, 50939 Köln, Germany. [⊥]Current address: Center for Integrated Nanotechnologies, Los Alamos National Laboratory, Los Alamos, NM, United States.

ABSTRACT Photoluminescence quantum yields and nonradiative decay of the excitonic S_1 state in length fractionated (6,5) single-wall carbon nanotubes (SWNTs) are studied by continuous wave and time-resolved fluorescence spectroscopy. The experimental data are modeled by diffusion limited contact quenching of excitons at stationary quenching sites including tube ends. A combined analysis of the time-resolved photoluminescence decay and the length dependence of photoluminescence quantum yields (PL QYs) from SWNTs in sodium cholate suspensions allows to determine the exciton diffusion coefficient $D = 10.7 \pm 0.4$ cm^{2}s^{-1} and lifetime τ_{PL} for long tubes of 20 ± 1 ps. PL quantum yields Φ_{PL} are found to scale with the inverse diffusion coefficient and the square of the mean quenching site distance, here $l_d = 120 \pm 25$ nm. The results suggest that low PL QYs of SWNTs are due to the combination of high-diffusive exciton mobility with the presence of only a few quenching sites.

KEYWORDS: carbon nanotubes · photoluminescence · spectroscopy · exciton · semiconductor · one-dimensional

The rates of energy transport and nonradiative decay in photonic or other types of devices are crucial for their performance.[1,2] A better understanding of the underlying microscopic phenomena is thus essential in determining the performance of the materials in question and may indicate fundamental performance limitations, while allowing at the same time to suggest the means by which figures of merit can be improved.[1]

The apparent dominance of nonradiative over radiative decay from semiconducting carbon nanotubes (SWNTs) and the associated low photoluminescence quantum yields (PL QYs) on the order of $10^{-4}-10^{-2}$ have been a particular challenge in the field of nanotube optics[3−8] and with the emergence of reports of significantly higher PL QYs up to 20% have also become more controversially debated.[9−11] Variations of PL QYs of carbon nanotubes in suspension or as vacuum-suspended individuals depend on a number of extrinsic parameters, such as the surfactant type used for dispersion, environmental pH, and type of nanotube synthesis. Some of the effects are expected to depend on the surfactant and molecular adsorption and the strength and type of interaction by which various molecular species interact with tubes,[12−14] while others are linked to physical effects, such as the role of dielectric screening for the interaction of charges with one another.[15] Environmental variability has also been found to affect the dynamics of optically excited states in SWNTs[16,17] and is likely to have an effect on other photophysical properties like the rate of ground-state recovery,[18] exciton size,[19] or exciton diffusion.[20,22]

Despite of the importance of nonradiative decay for SWNT photophysics, however, there appears to be no comprehensive kinetic model which can at the same time account for the small overall PL QYs, for effects like stepwise quenching by single-molecule reactions[20,23] and for the tube length dependence of PL QYs[8] while bearing recently proposed quenching by local doping in mind.[24,25]

Here, we present a kinetic model that attempts to reconcile the aforementioned experimental observations with our current understanding of exciton quenching. The model is based on the notion of diffusive exciton transport to localized quenching sites located on the tubes and at their ends. Specifically, the PL QY of excitons whose motion is governed by the diffusion coefficient D in the presence of a defect concentration $[Q]$ is found to scale as $\Phi_{PL} \propto [Q]^{-2}D^{-1}$. The exciton diffusion coefficient for the samples studied here of 10.7 ± 0.4 cm^{2}s^{-1} is 2−4 orders of magnitude higher than typical exciton diffusion coefficients in organic semiconductors[26,27] and thus explains the high sensitivity of PL from SWNTs

*Address correspondence to tobias.hertel@uni-wuerzburg.de

Received for review July 12, 2010 and accepted November 15, 2010.

Published online November 24, 2010. 10.1021/nn101612b

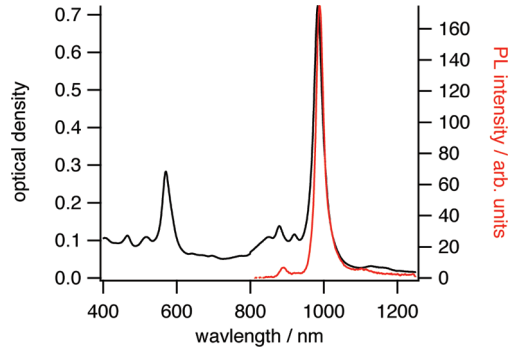

Figure 1. Absorption (black line, left axis) and emission spectrum (red line, right axis) of a length and chirality fractionated nanotube suspension. The spectrum is dominated by the S_1 and S_2 features of the most abundant (6,5) tube species.

to the presence of quenching sites as well as their notoriously low overall photoluminescence quantum yields.

RESULTS

Length selected SWNT samples are prepared from CoMoCat SG65 nanotube soot by a two-step process. The first step aims at chirality and the second step aims at length selection by density gradient and zonal ultracentrifugation, respectively.[6,28−31] This yields chirality- and length-sorted colloidal suspensions with an excess of 80% of all semiconducting tubes being of the (6,5) type and with less than 9% contamination by metallic tubes.[32]

Representative absorption and PL spectra of a (6,5) enriched suspension are shown in Figure 1. Length-fractionated samples are characterized at the ensemble level using fluorescence correlation spectroscopy (FCS).[33] The FCS data yield similar length distributions to previous investigations by atomic force microscopy (AFM) imaging and dynamic light scattering.[30,31] Here, the PL intensity autocorrelation fit function $g_2(\tau) = g_D(\tau)g_R(\tau)$ used for data analysis of rod diffusion depends on rod length and diameter and can be written as a product of the diffusional and rotational correlation functions $g_D(\tau)$ and $g_R(\tau)$, respectively.[33] A series of FCS spectra is shown in Figure 2 along with the best fit to each data set.

The time scale for rotational diffusion of molecules is typically orders of magnitude smaller than translational correlation times and thus frequently does not need to be considered in conventional FCS spectroscopy. For larger rod-like particles, such as the SWNTs studied here, however, characteristic time scales for rotational and diffusional autocorrelation functions become similar and have to be fit simultaneously to the FCS data. Here, we use the hydrodynamic stick theory which describes the dependence of both correlation times on rod length and diameter (see ref 33 and references therein). For our analysis we assume the diameter of the fully hydrated SWNT micelles to be 5 nm in accordance with analytical ultracentrifugation data.[34]

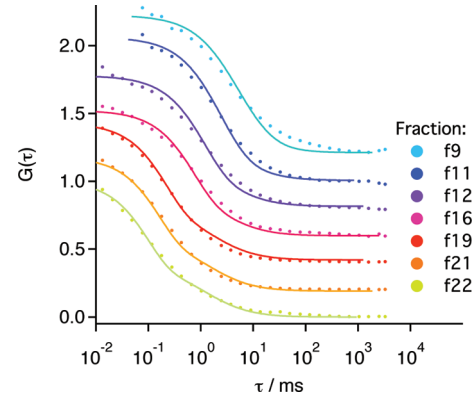

Figure 2. Fluorescence correlation spectra of length fractionated samples with lengths ranging from 190 up to 950 nm. Dots represent experimental data, and solid lines represent the results of a simultaneous fit of diffusional and rotational autocorrelation functions.

The fit routine adjusts tube length for best agreement with experimental FCS results.

Absolute photoluminescence quantum yields are determined from absorption and emission spectra, such as the ones shown in Figure 1. Emission intensities and PL QYs are referenced to Styryl 13, with its nearly ideal match of absorption and emission wavelengths to the S_1 and S_2 exciton transitions of (6,5) SWNTs studied here.[6] The PL QY of Styril 13 of 3.5% was determined using an integrating sphere. This is somewhat higher than the Styryl 13 PL QY of 1.4% recently reported by Stuerzl *et al.*[35] Such discrepancies are possibly due to differences of batch to batch sample or solvent quality, aging, and photoinduced degradation of the dye.

The resulting length dependence of PL QYs is shown in Figure 3. The PL QY increases gradually from 0.4% for SWNTs of 190 nm in length to about 1.0% for tubes with a length of 950 nm. Similar behavior was recently observed for lengths ranging up to 450 nm as reported by Rajan *et al.*[8] However, saturation of PL QYs could not be observed in the report by Rajan *et al.* due to tube lengths being limited to below 450 nm. The samples available for this study thus allow a more detailed investigation of the mechanism underlying the length de-

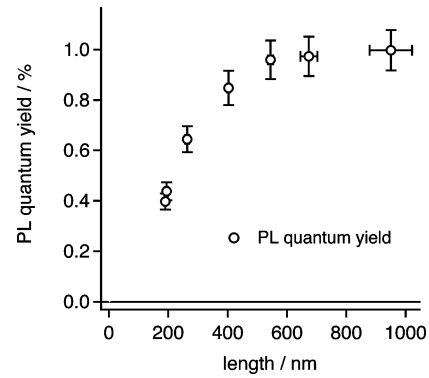

Figure 3. Length dependence of photoluminescence quantum yields for length-fractionated nanotube samples.

pendence of PL quantum yields. The kinetic model discussed in the following will be based on the notion of diffusion limited bimolecular contact quenching in one-dimensional systems (see for example references 36 and 37).

Diffusion Limited Exciton Quenching. Intentional doping is known to quench nanotube PL,[39,40] an effect whose local character has recently been demonstrated by monitoring of single-molecule reactions on individual SWNTs by PL microscopy.[20,23] Localized charge transfer and Fermi level shifts by dopants are thus believed to generate quenching sites that can lead to efficient nonradiative relaxation in SWNTs. Multiphonon decay (MPD), on the other hand, is the dominant mechanism for nonradiative deactivation in aromatic systems but has been estimated to be 2−3 orders of magnitude less efficient than dopant-induced quenching in SWNTs[24] and is thus been neglected in the present model. The present treatment should therefore be reasonable as long as quantum yields remain well below 10%. Quenching at tube ends is likewise considered to be a potential nonradiative decay channel,[8,41] owing to the higher reactivity and susceptibility of nanotube ends to chemical attack. The detailed mechanism of quenching is still discussed, and different models, such as phonon-assisted indirect ionization[24] or direct resonant dissociation,[25] have recently been put forward.

The model proposed in the following neglects radiative or other nonlocal decay mechanisms and discusses small PL quantum yields solely in terms of a mechanism based on localized de-excitation. Neglecting radiative decay and using a diffusion limited decay mechanism appears justified if the corresponding PL lifetime-based diffusion length $l_{d,PL}$ is much smaller than the corresponding radiative diffusion length $l_{d,rad}$. For PL lifetime limited exciton transport to be about 1 order of magnitude slower than the corresponding radiatively limited exciton transport in the absence of nonradiative decay thus requires PL QYs not to exceed a few percent.

Moreover, the diffusion of excitons is expected to be one-dimensional because the characteristic electron−hole pair separation of about 2.0 nm exceeds the tube diameter.[15,19,21] Once an exciton reaches a quenching site it is assumed to decay with high probability, *i.e.*, the use of the term contact quenching.

The kinetics of diffusion limited contact quenching (DLCQ) can then be described as a reaction of mobile excitons A^* with stationary quenching sites Q according to the generic bimolecular reaction mechanism:

$$A^* + Q \rightarrow A + Q \qquad (1)$$

where A represents the quenched exciton state. The quenching site concentration $[Q] = d_q^{-1}$ in m^{-1} as determined by the average quenching site distance d_q is assumed to remain constant. The change of the exciton population $d[A^*]/dt$ (in $m^{-1}s^{-1}$) is determined by the combined effects of radiative and nonradiative decay with characteristic rate constants k_{rad} and k_{nr}, respectively:

$$\frac{d[A^*]}{dt} = -k_{rad}[A^*] - k_{nr}[A^*][Q] \qquad (2)$$

Radiative decay is characterized by the radiative lifetime $\tau_{rad} = k_{rad}^{-1}$ which, in the absence of other decay mechanisms, leads to monoexponential decay of the exciton population. Nonradiative reaction kinetics on the other hand can lead to both monoexponential decay as well as more complex behavior. For time-independent rate constants, however, nonradiative decay is monoexponential and gives rise to a characteristic photoluminescence lifetime $\tau_{PL} = (k_{rad} + k_{nr})^{-1}$.

The number of photons emitted after excitation can be written as $N_{PL} = L[A^*]\tau_{PL}/\tau_{rad}$, where L is the total length of tubes in the sample. For purely radiative decay, the number of emitted photons would equal the number of absorbed photons $N_{abs} = N_{rad} = L[A^*]$. If nonradiative decay can be characterized by an exponential decrease of the excited-state concentration, then the PL QY can be written as $\Phi_{PL} = \tau_{PL}/\tau_{rad}$, the ratio of photoluminescence and radiative decay times. If nonradiative decay is nonexponential, however, we need to use the ratio of emitted over absorbed photons $\Phi_{PL} = N_{PL}/N_{abs}$.

The rate constant for diffusion limited contact quenching $k_{nr} = k_{nr}(t)$ is time dependent and scales with the exciton diffusion coefficient D and time t:[36,37]

$$k_{nr}(t) = \sqrt{\frac{D}{\pi t}} \qquad (3)$$

For small PL quantum yields Φ_{PL}, the decay of the excited-state concentration $[A^*](t)$ is then given by a stretched exponential or Kohlrausch function:[36]

$$[A^*](t) = [A^*]_0 \exp[-(t/\tau_0)^{1/2}] \qquad (4)$$

where $\tau_0 = \pi/(4D[Q]^2)$ is a characteristic time scale, and $[A^*]_0$ is the initial concentration of excited states.[36] The number of emitted photons is then obtained from integration of the population dynamics in eq 4 over time which, in the limit of negligible radiative deactivation, *e.g.*, small quantum yields, becomes

$$N_{PL} = \frac{L[A^*]_0\pi}{2D[Q]^2\tau_{rad}} \qquad (5)$$

The resulting PL QY Φ_{PL} is then given by the simple expression:

$$\Phi_{PL} = \frac{N_{PL}}{N_{abs}} = \frac{\pi}{2[Q]^2 D\tau_{rad}} \qquad (6)$$

where N_{abs} is obtained from integration of the dynamics underlying eq 2 over time using the fact that the

number of emitted N_{rad} and absorbed photons N_{abs} are identical for purely radiative decay.

It is noteworthy to point out the scaling of the PL QY with D^{-1} and with d_q^2. Within this model the exciton diffusion length l_d takes on the simple form:

$$l_d = \sqrt{2D\tilde{\tau}_{PL}} = d_q\sqrt{\pi} \quad (7)$$

with d_q being the average 'bulk' quenching site distance in the absence of end quenching, and $\tilde{\tau}_{PL}$ refers to the effective lifetime of a stretched exponential decay obtained from $\tilde{\tau}_{PL} = \Phi_{PL}\tau_{rad}$.

The length dependence of PL QYs is now obtained from eq 7 by treating end quenching on the same footing as the 'bulk' quenching discussed above. Here, ends are accounted for by adding one full bulk quenching site because each end is accessible from one side only. The effective quenching site concentration for a tube of length l is thus increased by one site per tube length and becomes $[Q] = (d_q^{-1} + l^{-1})$. This is illustrated schematically in Figure 4.

The length dependence of the PL QY in the limit of small overall quantum yields then becomes

$$\Phi_{PL}(l) = \frac{\pi}{2(d_q^{-1} + l^{-1})^2 D\tau_{rad}} \quad (8)$$

In Figure 5 we plot normalized length dependencies from eq 8 for hypothetical quenching site distances ranging from 25 to 400 nm. The strong dependence of PL QYs on quenching site concentration will provide high accuracy in the determination of average site distances. From eq eq 8 we also find that the average quenching site distance can be expressed in terms of $l_{1/2}$, the tube length at which the PL QY is at half its saturation value and becomes $d_q = (\sqrt{2} - 1)l_{1/2} \approx 0.4 \cdot l_{1/2}$.

A fit of eq 8 to experimental data now allows to determine the average quenching site distance as well as $D\tau_{rad}$, the product of diffusion coefficient and radiative lifetime. Determination of the diffusion coefficient thus requires knowledge of the radiative lifetime which is here obtained from a PL lifetime measurement using time-correlated single photon counting (TCSPC) in combination with the known PL QY. The PL decay of a sample with an average tube length of 950 nm is shown in Figure 6 for resonant excitation of the second subband exciton of (6,5) SWNTs at 570 nm.

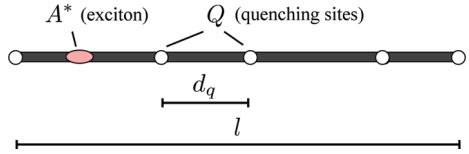

Figure 4. Schematic illustration of a SWNT with bulk and end quenching. The bulk-quenching site concentration is given by the average distance d_q. Within our model, the tube ends represent additional quenching sites whose concentration depends on the average tube length l.

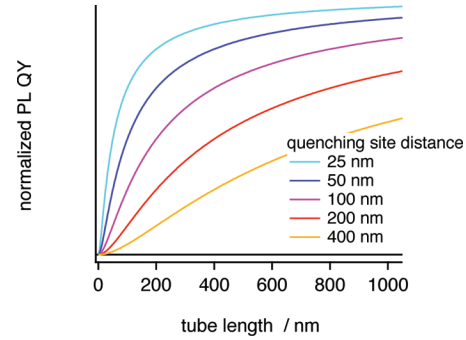

Figure 5. Predicted dependence of PL quantum yields on tube length and quenching site distance.

The effective PL lifetimes $\tilde{\tau}_{PL}$ of samples with SWNT lengths between 190 and 950 nm range from 9 to 15 ps and are summarized in Figure 7 along with the PL QY data from Figure 3.

The length dependence of PL lifetimes obtained from eq 8 has the same functional form as eq 8 and, in the limit of small overall quantum yields, becomes

$$\tilde{\tau}_{PL} = \frac{\pi}{2(d_q^{-1} + l^{-1})^2 D} \quad (9)$$

A simultaneous fit of the length dependence of PL QYs and effective lifetimes to the diffusion limited contact quenching model using eqs 8 and 9 (Figure 7) yield an average quenching site distance $d_q = 120 \pm 25$ nm. The corresponding exciton diffusion length $l_d = d_q\sqrt{\pi}$ is 210 $\pm$ 40 nm. For very long tubes the PL quantum yield is then expected to level off at 1.3%, while the PL lifetime is expected to reach a maximum of 20 $\pm$ 1 ps. This corresponds to a radiative lifetime $\tau_{rad} = 1.6 \pm 0.3$ ns and an exciton diffusion coefficient $D = 10.7 \pm 0.4$ cm^{2}s^{-1}.

One-dimensional mean free path diffusion theory can now be used to relate the diffusion coefficient D to the exciton dephasing time τ_φ. This is done by association of the exciton dephasing time with momentum randomizing interactions with the static or dynamic potential variations in the exciton potential energy land-

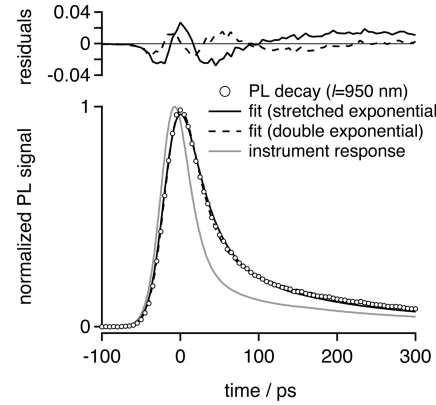

Figure 6. PL decay measured for a (6,5) enriched sample with an average SWNT length of 950 nm. The (6,5) tubes are resonantly excited at 570 nm with sub ps impulses from a Ti:sapphire oscillator pumped photonic fiber.

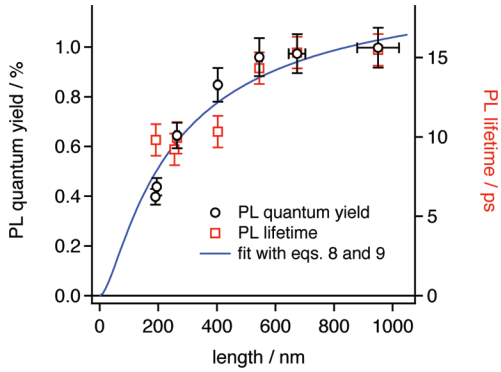

Figure 7. Summary of photoluminescence quantum yields (black circles, left axis), PL lifetimes (red squares, right axis) and the fit using eqs 8 and 9.

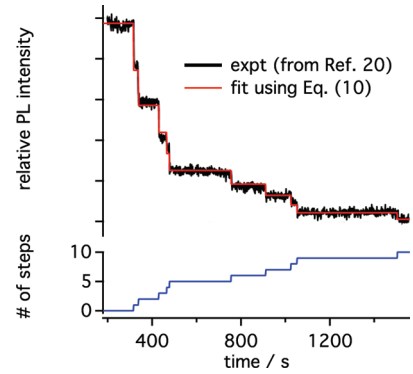

Figure 8. Stepwise quenching of PL induced by diazonium reactant (adapted from ref 20). The trace in the lower part of the figure is obtained from steps in the PL time trace and represents the number of additional quenching sites introduced during the experiment. The red line is a fit of eq 10 to the data. Reproduced with permission from ref 20. Copyright 2010 American Chemical Society.

scape with a characteristic time τ_{coll}. The dephasing time in turn can be compared to the experimentally accessible line width of the $S_1 \rightarrow S_0$ transition. The resulting one-dimensional diffusion coefficient can then be expressed as $D = (kT\tau_\varphi)/(4\pi m_{eff})$, where m_{eff} is the exciton effective mass, and T is the temperature.

If we use an exciton effective mass $m_{eff} \approx 0.01 m_e$[38] and a diffusion coefficient of $D \approx 11$ cm^{2}s^{-1}, then we obtain a room temperature dephasing time of 33 fs which, in the absence of significant lifetime broadening, corresponds to a homogeneous linewdith $\Gamma = \hbar/\tau_\varphi$ of 20 meV. This is in good agreement with the experimentally observed line width of the $S_1 \rightarrow S_0$ transition of 35 meV, some of which may have to be attributed to inhomogeneous broadening (see Figure 1). The diffusion coefficient obtained from our analysis of length-dependent PL QYs is thus in good agreement with estimates based on the homogeneous exciton transition line width.

Application to Single-Molecule PL Quenching. The diffusion-limited contact-quenching (DLCQ) model introduced above can also be applied to other situations involving exciton quenching. Single-tube PL spectroscopy, for example, has the potential to monitor individual doping events by the associated decrease of PL intensities.[23] In the following we briefly discuss how DLCQ can be used for comparison of the results from ensemble studies presented here, with observations in single-tube investigations, such as the ones by Cognet *et al.*,[23] where the authors monitor PL intensity changes during single-molecule reactions with individual SWNTs.

If doping introduces n additional quenching sites to a SWNT of length l, then the corresponding PL QYs in equation eq 8 becomes

$$\Phi_{PL} = \frac{\pi}{2(d_q^{-1} + (n+1)l^{-1})^2 D\tau_{rad}} \qquad (10)$$

In Figure 8a we reproduce stepwise quenching data from ref 20 as well as a fit to the data using eq 10. The number of steps required for the fit routine was determined manually by inspection of step occurrences and positions. A fit yields best agreement of eq 10 with experimental data for a l/d_q ratio of 9.0 $\pm$ 0.5. This implies that the average distance of quenching sites at the beginning of the experiment is one-ninth of the length of the 2.2 μm region monitored by the experiment.[49] This corresponds to an initial quenching site distance of 240 nm. Based on the number of steps in the time trace in Figure 8, the total number of quenching sites thus increases by about a factor of 2 toward the end of the experiment, and accordingly, the quenching site distance as well as the average exciton diffusion length are reduced by a factor of 2.

Using the above model we can also predict PL intensity changes $\Delta I_0/I$ induced by the addition of a single quenching site:

$$\frac{\Delta I_0}{I} = \frac{2(l/d_q + 3/2)}{(l/d_q + 2)^2} \qquad (11)$$

If the quenching at tube ends can be neglected, then we simply replace n with $n - 1$ and obtain:

$$\frac{\Delta I'_0}{I'} = \frac{2(\tilde{l}/d_q + 1/2)}{(\tilde{l}/d_q + 1)^2} \qquad (12)$$

The corresponding relationship between PL step height and l/d_q ratio is shown in Figure 9. From a reduction of the PL signal by about 15% by a single quenching site, as found by Siitonen *et al.*,[20] one can infer from Figure 9 that the l/d_q ratio should be 10, in close agree-

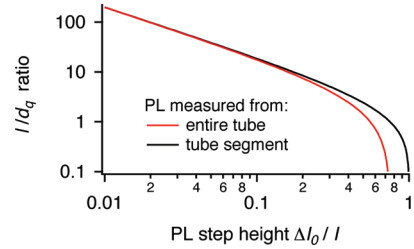

Figure 9. Predicted dependence of the l/d_q ratio on the step height in single tube quenching studies.

ment with the detailed analysis of several steps discussed above.

CONCLUSIONS

We have developed a kinetic model for diffusion limited contact quenching (DLCQ) of excited states in one-dimensional semiconductors, such as SWNTs. The model neglects nonlocal quenching effects, such as multiphonon decay, and thus applies to the limit of small PL quantum yields, on the order of a few percent. Within this model diffusion limited contact quenching is the dominant nonradiative decay mechanism. The diffusion length l_d frequently used for characterization of exciton dynamics becomes $l_d = d_q\sqrt{\pi}$ and is thus entirely limited by d_q, the average spacing of quenching sites. This may account for large variations of diffusion lengths found by different groups in different environments and for different sample types, ranging from 90 to 610 nm.[23,41−43] Moreover we find that the PL QYs scale with the square of the quenching site distance and inversely with the diffusion coefficient, *i.e.*, $\Phi_{PL} \propto d_q^2 D^{-1}$. By comparison, exciton diffusion constants in organic semiconductors are typically 2−4 orders of magnitude smaller.[26,27] The results also suggest that a reduction of quenching site concentration as well as a manipulation of diffusion coefficients by external fields or adsorbates should be very efficient in enhancing PL QYs.

In addition, the length dependence of PL QYs of SWNTs in aqueous suspension suggests that nanotube ends also quench PL efficiently. Average quenching site distances and diffusion coefficients of our samples are 120 ± 20 nm and 10.7 ± 0.4 cm^2s^{-1}, respectively. Time-resolved photoluminescence studies show that photoluminescence lifetimes of tubes with lengths from 190 to 950 nm increase from 9 to 15 ps and are expected to level off at 20 ps for very long tubes.

In short, the kinetic model presented here can account for the small overall PL QY of SWNTs, for effects like stepwise quenching by single molecule reactions, and for the tube-length dependence of PL QYs. The low PL QY can essentially be attributed to the combination of few localized quenching sites with high diffusive exciton mobilities. Future studies and kinetic modeling will have to investigate the role of nonlocal quenching or finite quenching probabilities on the overall nonradiative decay rates.

The unique value of the kinetic model introduced here lies in the simple parametrized form of the expressions derived for lifetime and quantum yield dependencies on the length of the system and on its bulk quenching site density. Future studies are expected to cast more light onto the predicted effect of the environment for exciton dynamics and exciton diffusion as well as on the possible effect of site character on quenching probabilities.

METHODS

Chirality and Length Fractionation. Chirality selection is performed using the process described by Arnold *et al.*[28] from SG65 CoMoCat starting material. This method yields (6,5) chirality enriched SWNTs with an excess of 80% of the semiconducting material belonging to the (6,5) species, as estimated from the spectral weight of different SWNT species in absorption spectra. In short, nanotube soot is ultrasonnicated in aqueous solution with a 4:1 sodium cholate (SC) to sodium dodecyl sulfate (SDS) surfactant mixture. The resulting heterogeneous mixture contains large and small aggregates as well as individual SWNT micelles.[6] Density gradient ultracentrifugation allows to separate isolated (6,5) tubes from aggregates and from SWNTs with other chiralities.

The resulting (6,5) enriched SWNT suspensions are separated by length using zonal fractionation.[30,31] The sensitivity of zonal fractionation to rod length is generally weak because, unlike for spherical particles, particle mass m_p and frictional coefficient f in the sedimentation coefficient $s = m_p f^{-1}(1 - \rho_s/\rho_p)$ are to a first-order approximation both expected to scale with rod length L removing any sensitivity of sedimentation to SWNT length.

Small, logarithmic corrections to the rod frictional coefficient $f = 6\pi\eta_s L/(2\ln(L/d) - \gamma_{||} - \gamma_{\perp})$, however, provide a small sensitivity to length and allow fractionation by zonal ultracentrifugation.[30,31] Here, ρ_s is the solvent, ρ_p the effective particle density, η_s the solvent viscosity, and $\gamma_{||}$ and $\gamma_{\perp}$ are weak aspect ratio dependent parameters.[33]

For zonal fractionation 0.5 mL of chirality enriched material from the first process with added 42 v% Optiprep density gradient medium is layered on top of two 0.5 mL high-density blocking layers of aqueous 2 w% SC solution with 50 and 66 w% Optiprep, respectively. The sample layer is covered with a 10 mL race layer of an aqueous 2 w% SC and 33 v% Optiprep solution with a density of 1.110−1.115 g cm^{-3}. The centrifuge vials with a diameter of 14 mm (Beckmann Ultraclear) are spun for 94 h in a SW 41 swinging bucket rotor at 12 krpm. Long and short (6,5) SWNTs float upward with sedimentation coefficients ranging from 18 to about 3 S, respectively.

SWNT Length Determination by Fluorescence Correlation Spectroscopy. Fluorescence correlation spectra were obtained for 543 nm excitation at 200 μW laser power using a commercial fluorescence microscope (Zeiss ConfoCor 2). A fit of autocorrelation curves to experimental data for different fractions is shown in Figure 2. The lengths obtained from the fit range from 190 to 950 nm. These results are in agreement with data obtained from an AFM study of length fractioned tubes by Fagan *et al.*[30,31] In the following we outline some of the details of our analysis of the FCS data.

Because of the low PL QYs of SWNTs used in this work of 0.4−1.0% and due to the low detector efficiency of Silicon avalanche photodiodes of about 1% in the emission range of (6,5) tubes, background noise, presumably from detector afterpulsing, contributes significantly to the intensity autocorrelation, in particular at smaller correlation times. To account for this signal contribution, we measured a background autocorrelation $g_b(\tau)$ (Figure 10) by using excitation of a blank sample and detecting residual light noise and its correlation with afterpulsing. The data are fit with the Igor Pro software package (Wavemetrics Inc.) using a triple exponential $g_b(\tau) = 1.3e^{-\tau/0.000151} + 1.06e^{-\tau/0.0012} + 0.25e^{-\tau/0.015}$. The model autocorrelation for analysis of SWNT FCS data thus contains two terms $g_2(\tau) = Ag_{SWNT}(\tau) + Bg_b(\tau)$.

Calibration of the confocal detection volume is achieved using Rhodamine 6G as reference dye with known photophysical properties. The detection volume is assumed to be elliptical in shape with the volume being given by $V = 4/3\pi S\omega_1^3$, where ω_1 is the laser beam radius in the focal plane,and $S = \omega_2/\omega_1$ specifies the ellipse aspect ratio with $2\omega_2$ being the length of the el-

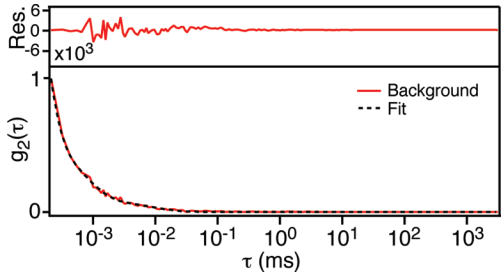

Figure 10. Background signal of Zeiss ConfoCor 2 due to afterpulsing.

lipse in the direction of the optical axis. The volume is determined using a 1 nM aqueous rhodamine 6G solution with 5 mM of NaCl. The diffusion coefficient of rhodamine 6G of $D_t = 280$ $\mu m^2\ s^{-1}$ [44] is used for calibration with the translational diffusion model of Krichevsky *et al.*:[47]

$$g_2(\tau) = \frac{1}{N}(1 - T + Te^{-\tau/\tau_T})\left(\frac{1}{1 + \frac{\tau}{\tau_t}}\right)\left(\frac{1}{1 + \frac{\tau}{S^2\tau_t}}\right)^{1/2} \quad (13)$$

where T is the fraction of molecules in their triplet state upon entering the confocal volume ($T = 1 - \eta$, where η is the photoluminescence quantum yield), N is the particle concentration, τ_T is the triplet lifetime, and τ_t is the characteristic translational diffusion time $\tau_t = \omega_1^2/(4D_t)$.

From the fit in Figure 11 we find $T = 0.141 \pm 0.003$, which is consistent with the quantum yield of rhodamine 6G in water $\eta = 0.90 \pm 0.02$,[45] $\tau_T = 1.7 \pm 0.1$ μs, which is consistent with the measured triplet lifetime of rhodamine 6G in water 2.0 ± 0.2 μs,[46] $N = 0.857 \pm 0.003$, $S = 10.0 \pm 0.4$, and $\tau_t = 53.1 \pm 0.6$ μs. The confocal radius is found to be $\omega_1 = 240 \pm 30$ nm. This corresponds to a confocal volume of $V = 0.61 \pm 0.07$ fL. The error in ω_1 introduces an uncertainty of 10% in determining the SWNT lengths.

Ensemble lengths are determined from model autocorrelation functions which need to account for both translational and rotational diffusive particle motion. Here we use well established rotational and translational rigid-rod autocorrelation functions (see ref 33 and references therein). The autocorrelation function used here for translational and rotational diffusion D_t and D_r is[33]

$$g_2(\tau) = A\left(\frac{1}{1 + \frac{\tau}{\tau_t}}\right)(1 + Re^{-\tau/\tau_r}) + Bg_b(\tau) \quad (14)$$

where $\tau_r = 1/(6D_r)$ is the rotational diffusion time, $\tau_t = \omega_1^2/(4D_t)$ is the translational diffusion time, and R is a factor related to the experimental geometry.[33] For the data in Figure 12 we obtain an ensemble length $l = 260 \pm 31$ nm and $R = 1.58 \pm 0.06$. R is consistent with the findings of Tsay *et al.*[33] who observe that R increases with the particle aspect ratio, from $R < 0.6$ for spherical nanoparticles to $0.6 \geq R > 1.0$ for lower aspect ratio nanorods to $R \geq 1.0$ for high-aspect ratio nanotubes studied here. Average tube lengths determined by analytical centrifugation for samples

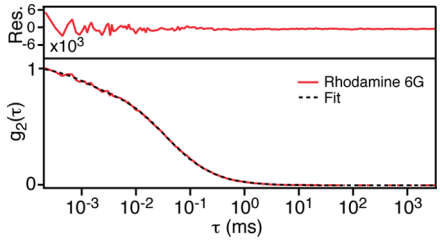

Figure 11. Fluorescence intensity autocorrelation for rhodamine 6G in water used to calibrate the confocal volume with the same excitation and detection conditions as for the data in Figure 10.

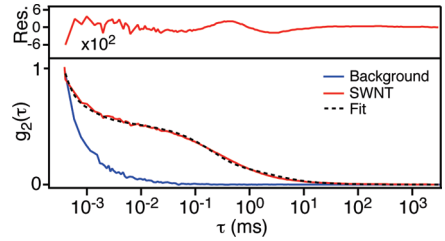

Figure 12. Fluorescence intensity autocorrelation and fit of an ensemble of (6,5) enriched tubes with the same excitation and detection conditions as Figure 1. The average length was found to be 260 ± 31 nm.

prepared under similar conditions to the ones used here are in agreement with our findings.[34]

Time-Resolved Photoluminescence Experiments. Resonant excitation of the second subband exciton in (6,5) SWNTs at 570 nm is here achieved using the band-pass filtered output of a photonic fiber driven by an 80 MHz Ti:sapphire oscillator. Care was taken to ensure that excitation densities are well below the fluence range of about 10^{14} cm^{-2}, where exciton−exciton annihilation starts to affect exciton dynamics.[48] The instrument response for data deconvolution was obtained for 980 nm light scattered of a polystyrene bead suspension.

Acknowledgment. The authors acknowledge stimulating discussions with M. Harra, A. Swan, A. Rajan, K. Schulten, D.A. Heller, M.S. Strano, and V. Perebeinos. We acknowledge B. Weisman and A. Siitonen for permission to use data from ref 20 for analysis and for providing additional information about the corresponding experiments.

REFERENCES AND NOTES

1. Forrest, S. A. The limits of photovoltaic cell efficiency. *MRS Bull.* **2005**, *30*, 28–32.
2. Halls, J. J. M.; Walsh, C. A.; Greenham, N. C.; Marseglia, E. A.; Friend, R. H.; Moratti, S. C.; Holmes, A. B. Efficient Photodiodes from Interpenetrating Polymer Networks. *Nature* **1995**, *375*, 490–500.
3. O'Connell, M. J.; Bachilo, S. M.; Huffman, C. B.; Moore, V. C.; Strano, M. S.; Haroz, E. H.; Rialon, K. L.; Boul, P. J.; Noon, W. H.; Kittrell, C. Band Gap Fluorescence from Individual Single-Walled Carbon Nanotubes. *Science* **2002**, *297*, 593–596.
4. Lebedkin, S.; Arnold, K.; Hennrich, F.; Renker, B.; Kappes, M. M. FTIR-Luminescence Mapping of Dispersed Single-Walled Carbon Nanotubes. *New J. Phys.* **2003**, *5*, 140.
5. Jones, M.; Engtrakul, C.; Metzger, W. K.; Ellingson, R. J.; Nozik, A. J.; Heben, M. J.; Rumbles, G. Analysis of Photoluminescence from Solubilized Single-Walled Carbon Nanotubes. *Phys. Rev. B: Condens. Matter Mater. Phys.* **2005**, *71*, 115426.
6. Crochet, J.; Clemens, M. S.; Hertel, T. Quantum Yield Heterogeneities of Aqueous Single-Wall Carbon Nanotube Suspensions. *J. Am. Chem. Soc.* **2007**, *129*, 8058–8059.
7. Crochet, J.; Clemens, M. S.; Hertel, T. Optical Properties of Structurally Sorted Single-Wall Carbon Nanotube Ensembles. *Phys. Status Solidi B* **2007**, *244*, 3964–3968.
8. Rajan, A.; Strano, M. S.; Heller, D. A.; Hertel, T.; Schulten, K. Length-Dependent Optical Effects in Single Walled Carbon Nanotubes. *J. Phys. Chem. B* **2008**, *112*, 6211–6213.
9. Ju, S.-Y.; Kopcha, W. P.; Papdimitrakopolous, F. Brightly Fluorescent Single-Walled Carbon Nanotubes *via* an Oxygen Excluding Surfactant Organisation. *Science* **2009**, *323*, 1319–1323.
10. Tsyboulski, D. A.; Rocha, J. D. R.; Bachilo, S. M.; Cognet, L.; Weisman, R. B. Structure-Dependent Fluorescence Efficiencies of Individual Single-Walled Carbon Nanotubes. *Nano Lett.* **2007**, *7*, 3080–3085.
11. Carlson, L. J.; Maccagnano, S. E.; Zeng, M.; Silcox, J.; Krauss, T. D. Fluorescence Efficiency of Individual Carbon Nanotubes. *Nano Lett.* **2007**, *7*, 3698–3703.

12. Ulbricht, H.; Kriebel, J.; Moos, G.; Hertel, T. Desorption Kinetics and Interaction of Xe with Single-Wall Carbon Nanotubes. *Chem. Phys. Lett.* **2002**, *363*, 252–260.
13. Ulbricht, H.; Moos, G.; Hertel, T. Interaction of Molecular Oxygen with Single-Wall Carbon Nanotubes. *Surf. Sci.* **2003**, *532*, 852–856.
14. Ulbricht, H.; Zacharia, R.; Cindir, N.; Hertel, T. Thermal Desorption of Gases from Graphite and Carbon Nanotubes. *Carbon* **2006**, *44*, 2931–2942.
15. Perebeinos, V.; Tersoff, J.; Avouris, P. Scaling of Excitons in Carbon Nanotubes. *Phys. Rev. Lett.* **2004**, *92*, 257402.
16. Hagen, A.; Steiner, M.; Raschke, M. B.; Lienau, C.; Hertel, T.; Qian, H.; Meixner, A. J.; Hartschuh, A. Exponential Decay Lifetimes of Excitons in Individual Single-Walled Carbon Nanotubes. *Phys. Rev. Lett.* **2005**, *95*, 197401.
17. Hertel, T.; Hagen, A.; Talalaev, V.; Arnold, K.; Hennrich, F.; Kappes, M.; Rosenthal, S; McBride, J.; Ulbricht, H.; Flahaut, E. Spectroscopy of Single- and Double-Wall Carbon Nanotubes in Different Environments. *Nano Lett.* **2005**, *5*, 511–514.
18. Zhu, Z.; Crochet, J.; Arnold, M. S.; Hersam, M. C.; Ulbricht, H.; Resasco, D.; Hertel, T. Pump-Probe Spectroscopy of Exciton Dynamics in (6,5) Carbon Nanotubes. *J. Phys. Chem. C* **2006**, *111*, 3831–3835.
19. Lüer, L.; Hoseinkhani, S.; Polli, D.; Crochet, J.; Hertel, T.; Lanzani, G. Size and Mobility of Excitons in (6,5) Carbon Nanotubes. *Nat. Phys.* **2009**, *5*, 54–58.
20. Siitonen, A. J.; Tsyboulski, D. A.; Bachilo, S. M.; Weisman, R. B. Surfactant Exciton Mobility in Single-Walled Carbon Nanotubes Studied by Single Molecule Reactions. *Nano Lett.* **2010**, *10*, 1595–1599.
21. Spataru, C. D.; Ismail-Beigi, S.; Benedict, L. X.; Louie, S. G. Excitonic Effects and Optical Spectra of Single-Walled Carbon Nanotubes. *Phys. Rev. Lett.* **2004**, *92*, 77402.
22. Murakami, Y.; Kono, J. Nonlinear Photoluminescence Excitation Spectroscopy of Carbon Nanotubes: Exploring the Upper Density Limit of One-Dimensional Excitons. *Phys. Rev. Lett.* **2009**, *102*, 037401.
23. Cognet, L.; Tsybouslki, D. A.; Rocha, J.-D. R.; Doyle, C. D.; Tour, J. M.; Weisman, R. B. Stepwise Quenching of Exciton Fluorescence in Carbon Nanotubes by Single-Molecule Reactions. *Science* **2007**, *316*, 1465–1468.
24. Perebeinos, V.; Avouris, P. Phonon and Electronic Nonradiative Decay Mechanisms of Excitons in Carbon Nanotubes. *Phys. Rev. Lett.* **2008**, *101*, 57401.
25. Hertel, T. *Photophysics in Carbon Nanotubes and Related Structures*. Guldi and Martin, VCH: Weinheim, Germany, 2010.
26. Lewis, A. J.; Ruseckas, A.; Gaudin, O. P. M.; Webster, G. R.; Burn, P. L.; Samuel, I. D. W. Singlet Exciton Diffusion in MEH-PPV Films Studied by Exciton-Exciton Annihilation. *Org. Electron.* **2006**, *7*, 452–456.
27. Mikhnenko, O. V.; Cordella, F.; Sieval, A. B.; Hummelen, J. C.; Blom, W. P. M.; Loi, M. A. Temperature Dependence of Exciton Diffusion in Conjugated Polymers. *J. Phys. Chem. B* **2008**, *112*, 11601–11604.
28. Arnold, M. S.; Stupp, S. I.; Hersam, M. S. Enrichment of Single-Walled Carbon Nanotubes by Diameter in Density Gradients. *Nano Lett.* **2005**, *5*, 713–718.
29. Arnold, M. S.; Green, A. A.; Hulvat, J. F.; Stupp, S. I.; Hersam, M. S. Sorting Carbon Nanotubes by Electronic Structure using Density Differentiation. *Nat. Nanotechnol.* **2006**, *1*, 80–85.
30. Fagan, J. A.; Simpson, J. R.; Bauer, B. J.; De Paoli Lacerda, S. H.; Becker, M. L.; Chun, J.; Migler, K. B.; Walker, A. R. H.; Hobbie, E. K. Length Dependent Optical Effects in Single-Wall Carbon Nanotubes. *J. Am. Chem. Soc.* **2007**, *129*, 10607–10612.
31. Fagan, J. A.; Becker, M. L.; Chun, J.; Hobbie, E. K. Length Fractionation of Carbon Nanotubes using Centrifugation. *Adv. Mater.* **2008**, *20*, 1609–1613.
32. Jorio, A.; Santos, P. A.; Ribeiro, H. B.; Fantini, C.; Souza, M.; Vieira, J. P. M.; Furtado, C. A.; Jiang, J.; Saito, R.; Balzano, L.; Resasco, D. E.; Pimenta, M. A. Quantifying Carbon-Nanotube Species with Resonance Raman Scattering. *Phys. Rev. B: Condens. Matter Mater. Phys.* **2005**, *72*, 075207.
33. Tsay, J. M.; Doose, S.; Weiss, S. Rotational and Translational Diffusion of Peptide-Coated CdSe/CdS/ZnS Nanorods Studied by Fluorescence Correlation. *J. Am. Chem. Soc.* **2006**, *128*, 1639–1647.
34. Arnold, M. S.; Suntivich, J.; Stupp, S. I.; Hersam, M. C. Hydrodynamic Characterization of Surfactant Encapsulated Carbon Nanotubes using an Analytical Ultracentrifuge. *ACS Nano* **2008**, *2*, 2291–2300.
35. Stuerzl, N.; Lebedkin, S.; Kappes, M. M. Revisiting the Laser Dye Styryl-13 as a Reference Near-Infrared Fluorophore: Implications for the Photoluminescence Quantum Yields of Semiconducting Single-Walled Carbon Nanotubes. *J. Phys. Chem. A* **2009**, *113*, 10238–10240.
36. Berberan-Santos, M. N.; Bodunov, E. N.; Valeur, B. Mathematical Functions for the Analysis of Luminescence Decays with Underlying Distributions 1. Kohlrausch Decay Function (Stretched Exponential). *Chem. Phys.* **2005**, *315*, 171–182.
37. Nau, W. M.; Wang, X. Biomolecular and Supramolecular Kinetics in the Submicrosecond Time Range: The Fluorazophore Approach. *ChemPhysChem* **2002**, *3*, 393–398.
38. Perebeinos, V.; Tersoff, J.; Avouris, P. Radiative Lifetime of Excitons in Carbon Nanotubes. *Nano Lett.* **2005**, *5*, 2495–2499.
39. Dukovic, G.; White, B. E.; Zhou, Z.; Wang, F.; Jockusch, S.; Steigerwald, M. L.; Heinz, T. F.; Friesner, R. A.; Turro, N. J.; Brus, L. E. Reversible Surface Oxidation and Efficient Luminescence Quenching in Semiconductor Single-Wall Carbon Nanotubes. *J. Am. Chem. Soc.* **2004**, *126*, 15269–15276.
40. Strano, M. S.; Huffman, C. B.; Moore, V. C.; OConnell, M. J.; Haroz, E. H.; Hubbard, J.; Miller, M.; Rialon, K.; Kittrell, C.; Ramesh. . Reversible, Band-Gap-Selective Protonation of Single-Walled Carbon Nanotubes in Solution. *J. Phys. Chem. B* **2003**, *107*, 6979–6985.
41. Georgi, C.; Böhmler, M.; Qian, H.; Novotny, L.; Hartschuh, A. Probing Exciton Propagation and Quenching in Carbon Nanotubes with Near-Field Optical Microscopy. *Phys. Status Solidi B* **2009**, *246*, 2683–2688.
42. Moritsubo, S.; Murai, T.; Shimada, T.; Murakami, Y.; Chisashi, S.; Maruyama, S.; Kato, Y. K. Exciton Diffusion in Air-Suspended Single-Walled Carbon Nanotubes; http://arxiv.org/abs/1003.0733v1.
43. Yoshikawa, K.; Matsuda, K.; Kanemitsu, Y. Exciton Transport in Suspended Single Carbon Nanotubes Studied by Photoluminescence Imaging Spectroscopy. *J. Phys. Chem. C* **2010**, *114*, 4353–4356.
44. Magde, D.; Elson, E. L.; Webb, W. W. Fluorescence Correlation Spectroscopy 2. Experimental Realization. *Biopolymers* **1974**, *13*, 29–61.
45. Magde, D.; Wong, R.; Seybold, P. G. Fluorescence Quantum Yields and their Relation to Lifetimes of Rhodamine 6G and Fluorescein in Nine Solvents: Improved Absolute Standards for Quantum Yields. *Photochem. Photobiol.* **2002**, *75*, 327–334.
46. Widengren, J.; Mets, U.; Rigler, R. Fluorescence Correlation Spectroscopy of Triplet States in Solution: A Theoretical and Experimental Study. *J. Phys. Chem.* **1995**, *99*, 13368–13379.
47. Krichevski, O; Bonnet, G. Fluorescence Correlation Spectroscopy: The Technique and its Applications. *Rev. Prog. Phys.* **2002**, *65*, 251–297.
48. Wang, F.; Dukovic, G.; Brus, L. E.; Heinz, T. F. Time-Resolved Fluorescence of Carbon Nanotubes and its Implication for Radiative Lifetimes. *Phys. Rev. Lett.* **2004**, *92*, 177401.
49. Siitonen, A. University of Jyväskylä, Finland, Private communication, 2010.